On-shell parameter fixing in the quark-meson model

Prabal Adhikari,[1,*] Jens O. Andersen,[2,3,†] and Patrick Kneschke[4,‡]

[1] *St. Olaf College, Physics Department, 1520 St. Olaf Avenue, Northfield, MN 55057, USA*
[2] *Department of Physics, Faculty of Natural Sciences, NTNU, Norwegian University of Science and Technology, Høgskoleringen 5, N-7491 Trondheim, Norway*
[3] *Niels Bohr International Academy, Blegdamsvej 17, Copenhagen 2100, Denmark*
[4] *Faculty of Science and Technology, University of Stavanger, N-4036 Stavanger, Norway*

(Dated: June 1, 2017)

The quark-meson model is often used as an effective low-energy model for QCD to study the chiral transition at finite temperature T and baryon chemical potential μ_B. The parameters in the quark-meson model can be found by expressing them in terms of the sigma mass m_σ, the pion mass m_π, the constituent quark mass m_q and the pion decay constant f_π. In practice, this matching is done at tree level, which is inconsistent once loop effects of the effective potential are taken into account. We show how to properly perform the matching in the quark-meson model by using the on-shell and the modified minimal subtraction renormalization schemes relating the physical masses and the pion decay constant to the running mass parameter and couplings. We map out the phase diagram in the μ_B–T plane and compare our results with other approximations.

I. INTRODUCTION

The first phase diagram of quantum chromodynamics (QCD) appeared in the 1970s, where it was suggested that it consists of a confined low-temperature phase of hadrons and a deconfined high-temperature phase of quarks and gluons. Since the appearance of this phase diagram, large efforts have been made to map it out in detail. The only existing first-principles method used to calculate the properties of finite-temperature QCD below the chiral transition is lattice simulation. However, due to the sign problem, it is difficult to perform lattice simulations at finite baryon chemical potential. Mapping out the phase diagram is therefore based on model calculations, in particular in the region of low temperature and large baryon chemical potential. See Refs. [1, 2] for reviews.

The $O(4)$-symmetric linear sigma model (LSM) is probably the simplest low-energy model of QCD. The degrees of freedom are the pions and the sigma particle. Often this model is augmented by an isospin doublet of fermions. In the old days, the fermionic doublet was identified with the neutron and proton. Now the isospin doublet consists of a u and a d quark. This extended model is referred to as the quark-meson (QM) model or the linear sigma model with quarks (LSMq). One may object to having both quark and mesonic degrees of freedom present at the same time. At very low temperatures, this is a valid objection since quarks are confined. This has led to the introduction of the Polyakov loop in these models in order to mimic confinement in QCD in a statistical sense by coupling the chiral models to a constant $SU(N_c)$ background gauge field A_μ^a [3]. One can express this background gauge field in terms of the complex-valued Polyakov loop variable Φ and consequently the effective potential becomes a function of the expectation value of the chiral condensate and the expectation value of the Polykov loop. The latter then serves as an approximate order parameter for confinement [4]. Finally, one adds the contribution to the free energy density from the gluons via a phenomenological Polyakov loop potential [5, 6]. At finite temperature and chemical potential, the (P)QM is often treated in the large-N_c limit which implies that one takes into account the one-loop correction to the effective potential from the fermions, but treats the mesonic degrees of freedom at tree level [7]. In some cases, one also neglects the vacuum fluctuations from the fermions and therefore renormalization issues altogether. This is sometimes referred to as the "no-sea" approximation.

The Lagrangian of the QM model has several parameters that can be expressed in terms of the physical quantities m_σ, m_π, m_q, and f_π. In this way one can fix the parameters of the model such that it reproduces the vacuum physics correctly. However, in most renormalization schemes, the tree-level relations between the parameters in the Lagrangian and physical quantities receive radiative corrections. It is therefore inconsistent to use tree-level values for these parameters in for example the calculation of the effective potential. While the on-shell parameters take their tree-level values, the parameters in $\overline{\rm MS}$ scheme are running and depend on the renormalization scale Λ, which has been introduced to keep the canonical dimension of the loop integrals. The idea is then to calculate the counterterms in the on-shell

* adhika1@stolaf.edu
† andersen@tf.phys.ntnu.no
‡ patrick.kneschke@uis.no

scheme as well as in the $\overline{\rm MS}$ scheme and relate the renormalized parameters in the two. The calculation of the effective potential is then carried out using (modified) minimal subtraction and the relations between the running parameters and the on-shell parameters, i.e. physical quantities are then used as input. This procedure has been well-known for decades by people doing loop calculations in the Standard Model, [8–11], but seems not to have been appreciated by practitioners in finite-temperature field theory, see however Refs. [12–16].

The paper is organized as follows. In Sec. II we briefly discuss the quark-meson model. We also calculate the self-energies and extract the counterterms in the on-shell scheme. In Sec. III, we derive relations between the physical quantities and the running parameters. In Sec. IV, we apply our results to the quark-meson model to map out the phase diagram in the μ–T plane. In the appendix, we list the integrals that are necessary in our calculations.

II. QUARK-MESON MODEL

In this section we briefly discuss the quark-meson model and calculate the one-loop self-energies in the large-N_c limit. We also derive the counterterms in the on-shell scheme.

A. Lagrangian and self-energies

The Lagrangian of the two-flavor quark-meson model in Minkowski space is

$$\begin{aligned}\mathcal{L} = &\frac{1}{2}\left[(\partial_\mu\sigma)^2 + (\partial_\mu\boldsymbol{\pi})^2\right] - \frac{1}{2}m^2(\sigma^2+\boldsymbol{\pi}^2)\\ &-\frac{\lambda}{24}(\sigma^2+\boldsymbol{\pi}^2)^2 + h\sigma + \bar\psi\left[i\partial\!\!\!/ + (\mu + \tfrac{1}{2}\tau_3\mu_I)\gamma^0\right.\\ &\left.-g(\sigma + i\gamma^5\boldsymbol{\tau}\cdot\boldsymbol{\pi})\right]\psi\,, \end{aligned} \tag{1}$$

where ψ is a color N_c-plet, a four-component Dirac spinor as well as a flavor doublet

$$\psi = \begin{pmatrix} u \\ d \end{pmatrix}\,. \tag{2}$$

Moreover, $\mu_B = 3\mu = \frac{3}{2}(\mu_u + \mu_d)$ and $\mu_I = (\mu_u - \mu_d)$ are the baryon and isospin chemical potentials expressed in terms of the quark chemical potentials μ_u and μ_d, τ_i $(i = 1, 2, 3)$ are the Pauli matrices in flavor space, and $\boldsymbol{\pi} = (\pi_1, \pi_2, \pi_3)$.

Apart from the global $SU(N_c)$ symmetry, the Lagrangian (1) has a $U(1)_B \times SU(2)_L \times SU(2)_R$ symmetry for $h = 0$ and a $U(1)_B \times SU(2)_V$ symmetry for $h \neq 0$. When $\mu_u \neq \mu_d$, this symmetry is reduced to $U(1)_B \times U_{I_3L}(1) \times U_{I_3R}(1)$ for $h = 0$ and $U(1)_B \times U_{I_3}(1)$ for $h \neq 0$. In the remainder of this paper we take $h = 0$, i.e. we work in the chiral limit. We also set $\mu_I = 0$.

In the vacuum, the sigma field acquires a nonzero expectation value ϕ_0. We can therefore write

$$\sigma = \phi_0 + \tilde\sigma\,, \tag{3}$$

where $\tilde\sigma$ is a quantum fluctuating field with a zero expectation value. At tree level, the masses of the sigma, the pion, and the quark are

$$m_\sigma^2 = m^2 + \frac{\lambda}{2}\phi_0^2\,, \tag{4}$$

$$m_\pi^2 = m^2 + \frac{\lambda}{6}\phi_0^2\,, \tag{5}$$

$$m_q = g\phi_0\,. \tag{6}$$

The tree-level potential $V_{\rm tree}$ is

$$V_{\rm tree} = \frac{1}{2}m^2\phi_0^2 + \frac{\lambda}{24}\phi_0^4\,, \tag{7}$$

and whose minimum is being identified with the pion decay constant f_π. The relations (4)–(6) can be solved with respect to the parameters of the Lagrangian (1). This yields

$$m^2 = -\frac{1}{2}\left(m_\sigma^2 - 3m_\pi^2\right)\,, \tag{8}$$

$$\lambda = 3\frac{(m_\sigma^2 - m_\pi^2)}{f_\pi^2}\,, \tag{9}$$

$$g^2 = \frac{m_q^2}{f_\pi^2}\,. \tag{10}$$

The Eqs. (8)–(10) are the parameters determined at tree level and are often used in practical calculations. However, as pointed out in the introduction, this is inconsistent in calculations that involve loop corrections unless one uses the on-shell renormalization scheme. In the on-shell scheme, the divergent loop integrals are regularized using dimensional regularization, but the counterterms are chosen differently from the minimal subtraction scheme. The counterterms in the on-shell scheme are chosen so that they exactly cancel the loop corrections to the self-energies and couplings evaluated on shell, and as a result the renormalized parameters are independent of the renormalization scale and satisfy the tree-level relations (8)–(10).

We need to introduce the counterterms for the parameters in the Lagrangian (1), δm^2, $\delta\lambda$, and δg^2, the wave function counterterms δZ_σ, δZ_π, and δZ_ψ. We then write

$$\sigma_{\rm B} = \sqrt{Z_\sigma}\sigma\,, \qquad \pi_{i\rm B} = \sqrt{Z_\pi}\pi_i\,, \tag{11}$$

$$\psi_{\rm B} = \sqrt{Z_\psi}\psi\,, \qquad m_{\rm B}^2 = Z_m m^2\,, \tag{12}$$

$$\lambda_{\rm B} = Z_\lambda\lambda\,, \qquad g_{\rm B}^2 = Z_{g^2}g^2\,, \tag{13}$$

where $Z_\sigma = 1 + \delta Z_\sigma$ etc. The counterterms δm^2, $\delta\lambda$, and δg^2 are expressed in terms of the counterterms δm_σ^2, δm_π^2, δm_q, and δf_π^2. From Eqs. (4)–(6), using Eqs. (11)–(13), one finds

$$\delta m^2 = -\frac{1}{2}\left(\delta m_\sigma^2 - 3\delta m_\pi^2\right) , \tag{14}$$

$$\delta\lambda = 3\frac{\delta m_\sigma^2 - \delta m_\pi^2}{f_\pi^2} - \lambda\frac{\delta f_\pi^2}{f_\pi^2} , \tag{15}$$

$$\delta g^2 = \frac{\delta m_q^2}{f_\pi^2} - g^2\frac{\delta f_\pi^2}{f_\pi^2} . \tag{16}$$

In the large-N_c limit $\delta m_q = 0$ and (16) directly relates δg^2 and δf_π^2. In this limit there are also no loop corrections to the pion-quark vertex, which means that the associated counterterms must cancel as well, leading to $\delta g^2 = -g^2\delta Z_\pi$. Together with (16) we can rewrite (15) as

$$\delta\lambda = 3\frac{\delta m_\sigma^2 - \delta m_\pi^2}{f_\pi^2} - \lambda\delta Z_\pi . \tag{17}$$

In the Feynman diagrams below, a solid line represents a sigma, a dashed line represents a pion, and the solid line with an arrow represents a quark. We work in the large-N_c limit, which implies that we are taking into account only fermion loops in the self-energies. The one-loop Feynman diagrams contributing to the self-energy of the sigma are shown in Fig. 1.

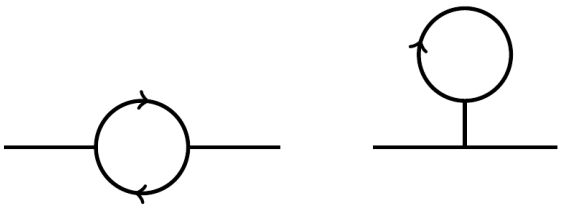

FIG. 1. One-loop self-energy diagrams for the sigma particle.

The corresponding contributions to the sigma self-energy are given by

$$\Sigma_\sigma(p^2) = -8g^2N_c\left[A(m_q^2) - \tfrac{1}{2}(p^2 - 4m_q^2)B(p^2)\right] + \frac{4\lambda g\phi_0 N_c m_q}{m_\sigma^2}A(m_q^2) , \tag{18}$$

where the integrals $A(m^2)$ and $B(p^2)$ are defined in Appendix A.

The diagrams contributing to the self-energy of the pion are shown in Fig. 2.

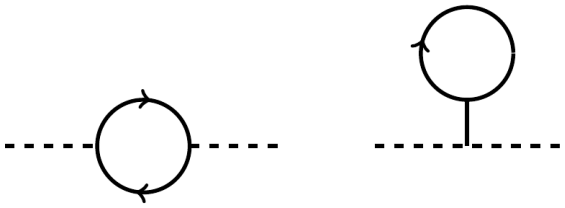

FIG. 2. One-loop self-energy diagrams for the pion.

The corresponding contributions to the pion self-energy are given by

$$\Sigma_\pi(p^2) = -8g^2N_c\left[A(m_q^2) - \tfrac{1}{2}p^2B(p^2)\right] + \frac{4\lambda g\phi_0 N_c m_q}{3m_\sigma^2}A(m_q^2) . \tag{19}$$

FIG. 3. Counterterm for the two-point functions for the sigma and pion.

The counterterm diagrams are shown in Fig. 3.

We do not need the quark self-energy since it is of order N_c^0. Thus $Z_\psi = 1$ and $\delta m_q = 0$ at this order.

The one-loop diagram that contributes to the one-point function together with the counterterm are shown in Fig. 4.

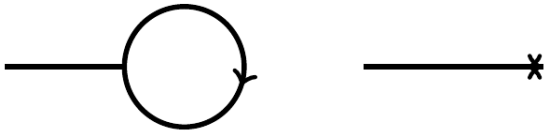

FIG. 4. Tadpole diagram for the sigma particle and the counterterm.

It reads

$$\delta\Gamma^{(1)} = -8N_c g m_q A(m_q^2) + i\delta t , \tag{20}$$

where δt is the counterterm for the tadpole, which can be expressed in terms of the other counterterms.

B. On-shell renormalization conditions

The inverse propagator for the sigma or pion can be written as

$$p^2 - m^2_{\sigma,\pi} - i\Sigma_{\sigma,\pi}(p^2)+\text{counterterms} \, . \tag{21}$$

In the on-shell scheme, the physical mass is equal to the renormalized mass in the Lagrangian, i.e. $m = m_{\rm pole}$.[1] Thus we can write

$$\Sigma^{\rm os}(p^2 = m^2_{\sigma,\pi})+\text{counterterms} = 0 \, . \tag{22}$$

The residue of the propagator on shell equals unity, which implies

$$\frac{\partial}{\partial p^2}\Sigma_{\sigma,\pi}(p^2)\Big|_{p^2=m^2_{\sigma,\pi}} +\text{counterterms} = 0 \, . \tag{23}$$

The equation of motion is that the one-point function vanishes. At tree level, the equation of motion is $t = m^2_\pi \phi_0 = 0$, and in the broken phase the pion mass is zero in accordance with Goldstone's theorem. The renormalization condition is then

$$\delta\Gamma^{(1)} = 0 \, . \tag{24}$$

The counterterms that correspond to Figs. 3 and 4 are given by

$$\Sigma^{\rm ct}_\sigma(p^2) = i\left[\delta Z_\sigma(p^2 - m^2_\sigma) - \delta m^2_\sigma\right] \, , \tag{25}$$

$$\Sigma^{\rm ct}_\pi(p^2) = i\left[\delta Z_\pi(p^2 - m^2_\pi) - \delta m^2_\pi\right] \, , \tag{26}$$

$$\Sigma^{\rm ct2}_\sigma = 3\Sigma^{\rm ct2}_\pi = \frac{i\lambda\phi_0^2}{2m^2_\sigma}\delta m^2_\pi \, , \tag{27}$$

$$\delta t = -\phi_0 \delta m^2_\pi \, . \tag{28}$$

The on-shell renormalization constants are given by the self-energies and their derivatives evaluated on shell. Combining Eqs. (22)–(26), we find

$$\delta m^2_\sigma = -i\Sigma_\sigma(m^2_\sigma) \, , \tag{29}$$

$$\delta m^2_\pi = -i\Sigma_\pi(0) \, , \tag{30}$$

$$\delta Z_\sigma = i\frac{\partial}{\partial p^2}\Sigma_\sigma(p^2)\Big|_{p^2=m^2_\sigma} \, , \tag{31}$$

$$\delta Z_\pi = i\frac{\partial}{\partial p^2}\Sigma_\pi(p^2)\Big|_{p^2=m^2_\pi} \, . \tag{32}$$

From Eqs. (18) and (19),[2] we find

$$\delta m^2_\sigma = 8ig^2 N_c\left[A(m^2_q) - \tfrac{1}{2}(m^2_\sigma - 4m^2_q)B(m^2_\sigma)\right] \, , \tag{33}$$

$$\delta m^2_\pi = 8ig^2 N_c A(m^2_q) \, , \tag{34}$$

$$\delta Z_\sigma = 4ig^2 N_c\left[B(m^2_\sigma) + (m^2_\sigma - 4m^2_q)B'(m^2_\sigma)\right] \, , \tag{35}$$

$$\delta Z_\pi = 4ig^2 N_c B(0) \, . \tag{36}$$

Using Eqs. (14)–(16), we find expressions for the counterterms $\delta m^2_{\rm OS}$, $\delta\lambda_{\rm OS}$, and $\delta g^2_{\rm OS}$,

$$\begin{aligned}\delta m^2_{\rm OS} &= 8ig^2 N_c\left[A(m^2_q) + \tfrac{1}{4}(m^2_\sigma - 4m^2_q)B_0(m^2_\sigma)\right] \\ &= = \delta m^2_{\rm div} + m^2\frac{4g^2N_c}{(4\pi)^2}\left[\log\left(\frac{\Lambda^2}{m^2_q}\right) + \frac{4m^2_q}{m^2_\sigma} + \left(1 - \frac{4m^2_q}{m^2_\sigma}\right)F(m^2_\sigma)\right] \, ,\end{aligned} \tag{37}$$

$$\begin{aligned}\delta\lambda_{\rm OS} &= -\frac{12ig^2N_c}{f^2_\pi}(m^2_\sigma - 4m^2_q)B(m^2_\sigma) - 4i\lambda g^2 N_c B(0) \\ &= \delta\lambda_{\rm div} + \frac{12g^2N_c}{(4\pi)^2}\frac{m^2_\sigma}{f^2_\pi}\left[\left(2 - \frac{4m^2_q}{m^2_\sigma}\right)\log\left(\frac{\Lambda^2}{m^2_q}\right) + \left(1 - \frac{4m^2_q}{m^2_\sigma}\right)F(m^2_\sigma)\right] \, ,\end{aligned} \tag{38}$$

$$\delta g^2_{\rm OS} = -4ig^4 N_c B(0) = \delta g^2_{\rm div} + \frac{4g^4N_c}{(4\pi)^2}\log\left(\frac{\Lambda^2}{m^2_q}\right) \, , \tag{39}$$

$$\delta Z^{\rm OS}_\sigma = \delta Z_{\sigma,\rm div} - \frac{4g^2N_c}{(4\pi)^2}\left[\log\left(\frac{\Lambda^2}{m^2_q}\right) + F(m^2_\sigma) + (m^2_\sigma - 4m^2_q)F'(m^2_\sigma)\right] \, , \tag{40}$$

$$\delta Z^{\rm OS}_\pi = \delta Z_{\pi,\rm div} - \frac{4g^2N_c}{(4\pi)^2}\log\left(\frac{\Lambda^2}{m^2_q}\right) \, , \tag{41}$$

[1] In defining the mass, we ignore the imaginary parts of the self-energy.

[2] The self-energies are without the tadpole contributions.

where $F(m^2)$ and $F'(m^2)$ are defined in Appendix A, and the divergent quantities are

$$\delta m^2_{\rm div} = m^2 \frac{4g^2 N_c}{(4\pi)^2 \epsilon} \,, \tag{42}$$

$$\delta \lambda_{\rm div} = \frac{8g^2 N_c}{(4\pi)^2 \epsilon} \left(\lambda - 6g^2\right) \,, \tag{43}$$

$$\delta g^2_{\rm div} = \frac{4g^4 N_c}{(4\pi)^2 \epsilon} \,, \tag{44}$$

$$\delta Z_{\sigma,{\rm div}} = \delta Z_{\pi,{\rm div}} = -\frac{4g^2 N_c}{(4\pi)^2 \epsilon} \,. \tag{45}$$

The divergent parts of the counterterms are the same in the two schemes, i.e. $\delta m^2_{\rm div} = \delta m^2_{\overline{\rm MS}}$ and so forth.

III. RELATIONS BETWEEN PARAMETERS IN THE TWO SCHEMES

Since the bare parameters are independent of the renormalization scheme, we can immediately write down the relations between the renormalized parameters in the on-shell and $\overline{\rm MS}$ schemes. We find

$$m^2_{\overline{\rm MS}} = \frac{Z^{\rm OS}_m}{Z^{\overline{\rm MS}}_m} m^2 \approx m^2 + \delta m^2_{\rm OS} - \delta m^2_{\overline{\rm MS}} \,, \tag{46}$$

$$\lambda_{\overline{\rm MS}} = \frac{Z^{\rm OS}_\lambda}{Z^{\overline{\rm MS}}_\lambda} \lambda \approx \lambda + \delta\lambda_{\rm OS} - \delta\lambda_{\overline{\rm MS}} \,, \tag{47}$$

$$g^2_{\overline{\rm MS}} = \frac{Z^{<{\rm OS}}_{g^2}}{Z^{\overline{\rm MS}}_{g^2}} g^2 \approx g^2 + \delta g^2_{\rm OS} - \delta g^2_{\overline{\rm MS}} \,. \tag{48}$$

Using Eqs. (37)–(39), we find the running parameters in the $\overline{\rm MS}$ scheme

$$\begin{aligned} m^2_{\overline{\rm MS}} &= m^2 + 8ig^2 N_c \left[A(m_q^2) + \tfrac{1}{4}(m_\sigma^2 - 4m_q^2) B(m_\sigma^2)\right] - \delta m^2_{\overline{\rm MS}} \\ &= -\tfrac{1}{2} m_\sigma^2 \left\{ 1 + \frac{4m_q^2 N_c}{(4\pi)^2 f_\pi^2} \left[\log\left(\frac{\Lambda^2}{m_q^2}\right) + \frac{4m_q^2}{m_\sigma^2} + \left(1 - \frac{4m_q^2}{m_\sigma^2}\right) F(m_\sigma^2) \right] \right\} \,, \end{aligned} \tag{49}$$

$$\begin{aligned} \lambda_{\overline{\rm MS}} &= \lambda - 4i\lambda g^2 N_c \left[\left(1 - \frac{4m_q^2}{m_\sigma^2}\right) B(m_\sigma^2) + B(0) \right] - \delta\lambda_{\overline{\rm MS}} \\ &= \frac{3m_\sigma^2}{f_\pi^2} \left\{ 1 + \frac{4m_q^2 N_c}{(4\pi)^2 f_\pi^2} \left[\left(2 - \frac{4m_q^2}{m_\sigma^2}\right) \log\left(\frac{\Lambda^2}{m_q^2}\right) + \left(1 - \frac{4m_q^2}{m_\sigma^2}\right) F(m_\sigma^2) \right] \right\} \,, \end{aligned} \tag{50}$$

$$\begin{aligned} g^2_{\overline{\rm MS}} &= g^2 - 4ig^4 N_c B(0) - \delta g^2_{\overline{\rm MS}} \\ &= \frac{m_q^2}{f_\pi^2} \left\{ 1 + \frac{4m_q^2 N_c}{(4\pi)^2 f_\pi^2} \log\left(\frac{\Lambda^2}{m_q^2}\right) \right\} \,, \end{aligned} \tag{51}$$

where the physical on-shell values are related to the meson and quark masses given by Eqs. (8)–(10).

The running parameters $m^2_{\overline{\rm MS}}(\Lambda)$, $\lambda_{\overline{\rm MS}}(\Lambda)$, and $g^2_{\overline{\rm MS}}(\Lambda)$ satisfy a set of renormalization group equations, which in the large-N_c limit are

$$\Lambda \frac{dm^2_{\overline{\rm MS}}(\Lambda)}{d\Lambda} = \frac{8m^2_{\overline{\rm MS}}(\Lambda) g^2_{\overline{\rm MS}}(\Lambda) N_c}{(4\pi)^2} \,, \tag{52}$$

$$\Lambda \frac{dg^2_{\overline{\rm MS}}(\Lambda)}{d\Lambda} = \frac{8g^4_{\overline{\rm MS}}(\Lambda) N_c}{(4\pi)^2} \,, \tag{53}$$

$$\Lambda \frac{d\lambda_{\overline{\rm MS}}(\Lambda)}{d\Lambda} = \frac{16 N_c}{(4\pi)^2} \left[\lambda_{\overline{\rm MS}}(\Lambda) g^2_{\overline{\rm MS}}(\Lambda) - 6 g^4_{\overline{\rm MS}}(\Lambda) \right] \,, \tag{54}$$

The solutions to Eqs. (52)–(54) are

$$m^2_{\overline{\rm MS}}(\Lambda) = \frac{m_0^2}{1 - \frac{4g_0^2 N_c}{(4\pi)^2} \log\frac{\Lambda^2}{m_q^2}} \,, \tag{55}$$

$$g^2_{\overline{\rm MS}}(\Lambda) = \frac{g_0^2}{1 - \frac{4g_0^2 N_c}{(4\pi)^2} \log\frac{\Lambda^2}{m_q^2}} \,, \tag{56}$$

$$\lambda_{\overline{\rm MS}}(\Lambda) = \frac{\lambda_0 - \frac{48 g_0^4 N_c}{(4\pi)^2} \log\frac{\Lambda^2}{m_q^2}}{\left(1 - \frac{4g_0^2 N_c}{(4\pi)^2} \log\frac{\Lambda^2}{m_q^2}\right)^2} \,, \tag{57}$$

where m_0^2, g_0^2, and λ_0 are the values of the running mass and couplings at the scale $\Lambda = m_q$. They are found by evaluating Eqs. (49)–(51) at this scale.

In the Nambu-Jona-Lasinio model, we have the relation $m_\sigma = 2m_q$ [18], while there is no such relation

between the sigma mass and quark mass in the quark-meson model. However, it is interesting to note that for $m_\sigma = 2m_q$, the tree-level relation $\lambda = 12g^2$ is valid at the one-loop level in the large-N_c limit; using $\lambda_0 = 3\frac{m_\sigma^2}{f_\pi^2} = 12g_0^2$, we find $\lambda_{\overline{\rm MS}}(\Lambda) = 12g^2_{\overline{\rm MS}}(\Lambda)$.

IV. RESULTS AND DISCUSSION

In this section, we calculate the one-loop effective potential and study the phase diagram. We are working in the large-N_c limit, which implies that only fermion loops are taken into account. This is often referred to as the mean-field approximation. The one-loop contribution to the effective potential is straightforward to calculate in this limit and reads

$$V_1 = -4N_c \sum\!\!\!\!\!\!\int_{\{P\}} \log\left[P^2 + \Delta^2\right] \,, \tag{58}$$

where the sum-integral is defined in Appendix A. After redefining the field ϕ_0 and renormalizing the mass parameter m^2 and coupling constants g^2 and λ, we find

$$\begin{aligned} V_{1-\rm loop} = {} & \frac{1}{2} m^2_{\overline{\rm MS}}(\Lambda) \frac{\Delta^2}{g^2_{\overline{\rm MS}}(\Lambda)} + \frac{\lambda_{\overline{\rm MS}}(\Lambda)}{24} \frac{\Delta^4}{g^4_{\overline{\rm MS}}(\Lambda)} + \frac{2N_c\Delta^4}{(4\pi)^2}\left[\log\frac{\Lambda^2}{\Delta^2} + \frac{3}{2}\right] \\ & -4N_c T \int_p \left\{ \log\left[1 + e^{-\beta(E-\mu)}\right] + \log\left[1 + e^{-\beta(E+\mu)}\right] \right\}, \end{aligned} \tag{59}$$

where $\mu = \mu_u = \mu_d$ is the quark chemical potential, and $E = \sqrt{p^2 + \Delta^2}$. Substituting the running parameters Eqs. (55)–(57) into Eq. (59), the effective potential becomes independent of the renormalization scale Λ and reads

$$\begin{aligned} V_{1-\rm loop} = {} & -\frac{1}{4} m_\sigma^2 f_\pi^2 \left\{ 1 + \frac{4m_q^2 N_c}{(4\pi)^2 f_\pi^2} \left[\left(1 - \frac{4m_q^2}{m_\sigma^2}\right) F(m_\sigma^2) + \frac{4m_q^2}{m_\sigma^2} \right] \right\} \frac{\Delta^2}{m_q^2} \\ & + \frac{1}{8} m_\sigma^2 f_\pi^2 \left\{ 1 - \frac{4m_q^2 N_c}{(4\pi)^2 f_\pi^2} \left[\frac{4m_q^2}{m_\sigma^2} \left(\log\left(\frac{\Delta^2}{m_q^2}\right) - \frac{3}{2} \right) - \left(1 - \frac{4m_q^2}{m_\sigma^2}\right) F(m_\sigma^2) \right] \right\} \frac{\Delta^4}{m_q^4} \\ & -4N_c T \int_p \left\{ \log\left[1 + e^{-\beta(E-\mu)}\right] + \log\left[1 + e^{-\beta(E+\mu)}\right] \right\}. \end{aligned} \tag{60}$$

In the remainder of the paper, we set $N_c = 3$. Moreover, the mass of the sigma particle is not known very accurately [17]. It is therefore common to vary it within the range of 400–800 MeV to study the effects on the phase diagram.

In Fig. 5, we show the normalized tree-level (dashed line) as well as the one-loop (solid line) effective potential in the vacuum ($\mu = T = 0$) as a function of Δ for $m_\sigma = 600$ MeV. This corresponds to the NJL relation between the sigma mass and the constituent quark mass, $m_\sigma = 2m_q$. Both potentials have a minimum at $\Delta = 300$ MeV, but the one-loop effective potential is significantly deeper.

In Fig. 6 we also show the normalized tree-level (dashed line) as well as the one-loop (solid line) effective potential in the vacuum ($\mu = T = 0$) as a function of Δ for $m_\sigma = 800$ MeV. Qualitatively, the potential looks the same as in Fig. 5.

In Fig. 7, we show the phase diagram in the μ–T plane for $m_\sigma = 600$ MeV. If one excludes the vacuum fluctuations of the fermions and hence ignores renormalization issues altogether, the model predicts a first-order transition in the entire μ–T plane. For vanishing chemical baryon potential μ, universality arguments suggest that it is second order [19], and strongly suggests that one should take the vacuum fluctuations of any model seriously [20–22]. Moreover, the first-order transition that starts at $T = 0$, ends at the tricritical point indicated by a red dot and located at $(\mu, T) = (303.24\ \text{MeV}, 55\ \text{MeV})$.

In Fig. 8, we show the phase diagram in the μ–T plane for $m_\sigma = 800$ MeV. The transition is now of second order in the entire μ–T plane, if one includes vacuum fluctuations and first order if they are neglected. For both values of m_σ, the critical temperature increases signif-

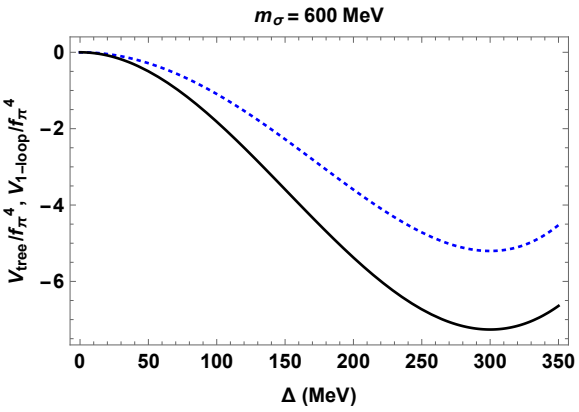

FIG. 5. Vacuum effective potential normalized to f_π^4 as a function of Δ for $m_\sigma = 600$ MeV. Dashed line is the tree-level potential and the solid line is the one-loop effective potential in the large-N_c limit.

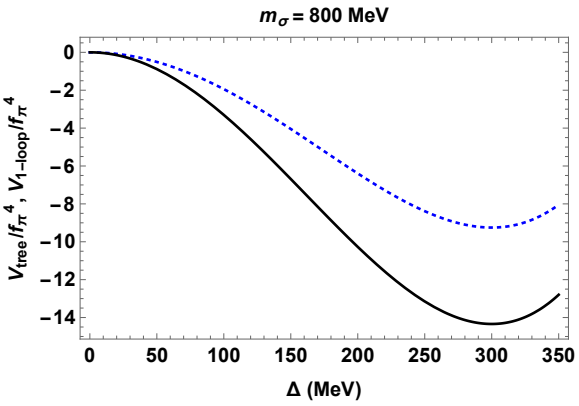

FIG. 6. Vacuum effective potential normalized to f_π^4 as a function of Δ for $m_\sigma = 800$ MeV. Dashed line is the tree-level potential and the solid line is the one-loop effective potential in the large-N_c limit.

icantly by including the vacuum fluctuations and one-loop corrections to the parameters of the Lagrangian (1). Our results for a sigma mass of 600 MeV and 800 MeV are in very good agreement with those of Ref. [16], where the authors use Pauli-Villars regularization and the pole mass definition to study the phase diagram of the QM model. There are a number of other studies of this model; however, a quantitative comparison is difficult since the curvature of the effective potential is used to define the sigma mass (see discussion below) or because matching is done at tree level. Qualitatively, the functional-renormalization group (FRG) study in Ref. [23] predicts a more complicated phase structure at low T. The second-order line starting at $\mu = 0$ ends at a

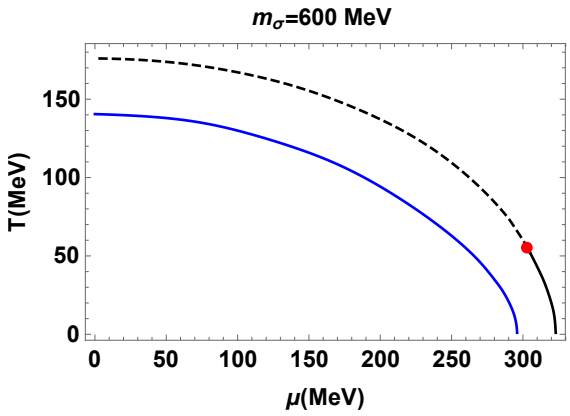

FIG. 7. The phase diagram in the μ–T plane for $m_\sigma = 600$ MeV. A dashed line indicates a second-order transition, while a solid indicates a first-order transition. The red dot shows the tricritical point. The blue solid line is phase boundary in the no-sea approximation.

tricritical point. The first-order transition bifurcates at larger values of μ where one of the branches is first order, while the second branch initially is first order and then second order. This more complicated structure may very well be related to the fact that the FRG includes mesonic fluctuations.

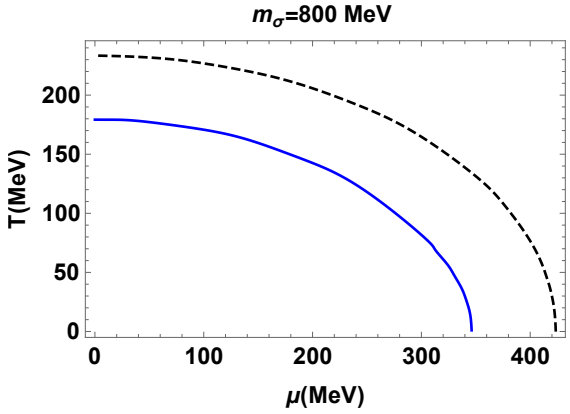

FIG. 8. The phase diagram in the μ–T plane for $m_\sigma = 800$ MeV. A dashed line indicates a second-order transition, while a solid indicates a first-order transition. The blue solid line is the phase boundary in the no-sea approximation.

A common, but incorrect definition of the sigma mass is the second derivative of the effective potential in the minimum. This is often referred to as the curvature mass. The effective potential is the generator of the n-point functions of the theory at vanishing external mo-

menta and so the curvature mass is equivalent to defining the sigma mass using the self-energy evaluated at vanishing momentum. The difference between the two masses is finite, but a priori difficult to quantify. In hot gauge theories, the correct way of defining the mass has a long history, and we emphasize that the pole definition is the physical and gauge invariant one [24, 25]. If different definitions of masses are used or if tree-level relations are applied at the loop level, one cannot compare different model predictions quantitatively. It is therefore important to determine the parameters in the Lagrangian in the correct way.

To summarize, we have calculated the running parameters m^2, λ, and g^2 at one loop by relating the $\overline{\rm MS}$ and on-shell schemes and the experimental values for the meson and quark masses and pion decay constant. We used this as input to the one-loop effective potential that was used to map out the phase diagram in the μ–T plane. We will present a more complete analysis including the Polyakov loop variable Φ and the possibility of inhomogeneous phases in a forthcoming publication [26]. The correct determination of the parameters in the quark-meson model should be useful in other contexts. For example, the $SU(3)$ quark-meson model has been used to study the phase diagram of QCD and quark stars.

ACKNOWLEDGMENTS

The authors would like to thank the Niels Bohr International Acedemy for its hospitality during the early stages of this work. J.O.A. would like to thank S. Carignano and M. Buballa for useful discussions.

INTEGRALS AND SUM INTEGRALS

The divergent loop integrals are regularized using dimensional regularization. We define the dimensionally regularized integrals by

$$\int_p = \left(\frac{e^{\gamma_E}\Lambda^2}{4\pi}\right)^\epsilon \int \frac{d^D p}{(2\pi)^D} \,, \tag{61}$$

where $D = 4-2\epsilon$, γ_E is the Euler-Mascheroni constant, and Λ is the renormalization scale associated with the $\overline{\rm MS}$ scheme. Specifically, we need the integrals

$$\begin{aligned} A(m^2) &= \int_p \frac{1}{p^2-m^2} \\ &= \frac{im^2}{(4\pi)^2}\left(\frac{\Lambda^2}{m^2}\right)^\epsilon \left[\frac{1}{\epsilon}+1\right] \,, \end{aligned} \tag{62}$$

$$\begin{aligned} B(p^2) &= \int_k \frac{1}{(k^2-m^2)[(k+p)^2-m^2]} \\ &= \frac{i}{(4\pi)^2}\left(\frac{\Lambda^2}{m^2}\right)^\epsilon \left[\frac{1}{\epsilon}+F(p^2)\right] \,, \end{aligned} \tag{63}$$

$$B'(p^2) = \frac{i}{(4\pi)^2}F'(p^2) \,, \tag{64}$$

where the functions q, $F(p^2)$, and $F'(p^2)$ are

$$q = \sqrt{\frac{4m^2}{p^2}-1} \,, \tag{65}$$

$$\begin{aligned} F(p^2) &= -\int_0^1 dx\, \log\left[\frac{p^2}{m^2}x(x-1)+1\right] \\ &= 2 - 2q\arctan\left(\tfrac{1}{q}\right) \,, \end{aligned} \tag{66}$$

$$F'(p^2) = \frac{4m^2 q}{p^2(4m^2-p^2)}\arctan\left(\tfrac{1}{q}\right) - \frac{1}{p^2} \,. \tag{67}$$

In the imaginary-time formalism for thermal field theory, a fermion has Euclidean 4-momentum $P = (P_0, \mathbf{p})$ with $P^2 = P_0^2 + \mathbf{p}^2$. The Euclidean energy P_0 has discrete values: $P_0 = (2n+1)\pi T + i\mu$, where n is an integer. Loop diagrams involve a sum over P_0 and an integral over spatial momenta p. With dimensional regularization, the integral is generalized to $d = 3-2\epsilon$ spatial dimensions. We define the dimensionally regularized sum-integral by

$$\sum\!\!\!\!\!\!\int_{\{P\}} = T\sum_{\{P_0\}}\int_p \,, \tag{68}$$

where Λ is the renormalization scale in the modified minimal subtraction scheme $\overline{\rm MS}$ and

$$\int_p = \left(\frac{e^{\gamma_E}\Lambda^2}{4\pi}\right)^\epsilon \int \frac{d^d p}{(2\pi)^d} \,. \tag{69}$$

Specifically, we need the sum-integral

$$I_0 = \sum\!\!\!\!\!\!\int_{\{P\}} \log\left[P^2+m^2\right] \,. \tag{70}$$

Summing over the Matsubara frequencies P_0, we obtain

$$\begin{aligned} I_0 = -\int_p \sqrt{p^2+m^2} - T\int_p \Big\{ &\log\left[1+e^{-\beta(E-\mu)}\right] \\ &+ \log\left[1+e^{-\beta(E+\mu)}\right]\Big\} \,. \end{aligned} \tag{71}$$

The first term is ultraviolet divergent and in dimensional regularization it reads

$$\int_p \sqrt{p^2+m^2} = -\frac{2m^4}{(4\pi)^2}\left(\frac{\Lambda^2}{m^2}\right)^{\epsilon}\left[\frac{1}{\epsilon}+\frac{3}{2}\right] \ . \quad (72)$$

---

[1] M. G. Alford, A. Schmitt, and K .Rajagopal, Rev. Mod. Phys. **80**, 1455 (2008),
[2] K. Fukushima, and T. Hatsuda, Rep. Prog. Phys. **74**, 014001 (2011).
[3] K. Fukushima, Phys. Lett. B **591**, 277 (2004).
[4] B. Svetitsky and L. G. Yaffe, Nucl. Phys. B **210**, 423 (1982).
[5] C. Ratti, M. A. Thaler, and W. Weise, Phys. Rev. D **73**, 014019 (2006).
[6] K. Fukushima, Phys. Rev. D **78**, 114019 (2008).
[7] O. Scavenuius, A. Mocsy, I. N. Mishustin, and D. H. Rischke, Phys. Rev. C **64**, 045202 (2001).
[8] A. Sirlin, Phys. Rev. D **22**, 971 (1980).
[9] A. Sirlin, Phys. Rev. D **29**, 89 (1984).
[10] M. Bohm, H. Spiesberger, and W. Hollik, Fortsch. Phys. **34**, 687 (1986).
[11] W Hollik, Fortsch. Phys. **38**, 165, (1990).
[12] K. Kajantie, M. Laine, K. Rummukainen, and M. E. Shaposhnikov Nucl. Phys. B **458**, 90 (1996).
[13] S. Chiku and T. Hatsuda, Phys. Rev. D **57**, 6 (1998).
[14] S. Chiku and T. Hatsuda, Phys. Rev. D **58**, 076001 (1998).
[15] Y. Hidaka, O. Morimatsu, and T. Nishikawa, Phys. Rev. D **67**, 056004 (2003).
[16] S. Carignano, M. Buballa, and W. Elkamhawy, Phys. Rev. D **94**, 034023 (2016).
[17] Particle data group, http://pdg.lbl.gov/2014/listings/rpp2014-list-f0-500.pdf.
[18] S. Klevansky, Rev. Mod. Phys. **64**, 649 (1992).
[19] R. D. Pisarski and F. Wilczek, Phys. Rev. D **29**, 338 (1984).
[20] V. Skokov, B. Friman, E. Nakano, K. Redlich, and B.-J. Schaefer, Phys. Rev. D **82**, 034029 (2010).
[21] R. Khan and L. T. Kyllingstad, AIP Conf. Proc. **1343**, 504 (2011).
[22] U. S. Gupta, V. K. Tiwari, Phys. Rev. D **85**, 014010 (2012).
[23] B.-J. Schaefer and J. Wambach, Nucl. Phys. A **757**, 479 (2005).
[24] R. Kobes, G. Kunstatter and A. Rebhan, Phys. Rev. Lett. **64**, 2992 (1990); Nucl. Phys. B **355** 1 (1991).
[25] A. K. Rebhan, Phys. Rev. D **48**, R3967 (1993).
[26] P. Adhikari, J. O. Andersen, and Patrick Kneschke, (to be published).